40. Paroush, Z. *et al. Cell* **79,** 805–815 (1994).
41. Komachi, K., Redd, M. J. & Johnson, A. D. *Genes Dev.* **8,** 2857–2867 (1994).
42. Tzamarias, D. & Struhl, K. *Genes Dev.* **9,** 821–831 (1995).
43. Hiebert, S. W., Chellappan, S. P., Horowitz, J. M. & Nevins, J. R. *Genes Dev.* **6,** 177–185 (1992).
44. Mangelsdorf, D. J. *et al. Cell* **66,** 555–561 (1991).
45. Willy, P. J. *et al. Genes Dev.* **9,** 1033–1045 (1995).
46. Koenig, R. J. *et al. Nature* **337,** 659–661 (1989).
47. Lazar, M. A., Hodin, R. A. & Chin, W. W. *Proc. natn. Acad. Sci. U.S.A.* **86,** 7771–7774 (1989).
48. Ayer, D. E., Lawrence, Q. A. & Eisenman, R. N. *Cell* **80,** 767–776 (1995).
49. Schreiber-Agus, N. *et al. Cell* **80,** 777–786 (1995).
50. Chen, J. D. & Evans, R. M. *Nature* **377,** 454–457 (1995).
51. Ingraham, H. A. *et al. Cell* **55,** 519–529 (1988).
52. Kurokawa, R. *et al. Nature* **371,** 528–531 (1994).

ACKNOWLEDGEMENTS. We thank R. Brent for advice and reagents, and B. Anderson for the mouse pituitary cDNA library. A.H. received postdoctoral support from the Deutsche Forschungsgemeinschaft (DFG) and the American Heart Association, T.H. from the DFG and the UC Breast Cancer Research Program, J.T. from the Medical Research Council of Canada, and A.R. from the NIH. M.G.R. is an investigator with HHMI. This research was supported by grants from the NIH to M.G.R. and C.K.G. and the US Army Breast Cancer Research Program.

LETTERS TO NATURE

Constraints on the origin of the Moon's atmosphere from observations during a lunar eclipse

Michael Mendillo & Jeffrey Baumgardner

Center for Space Physics and Department of Astronomy, Boston University, Boston, Massachusetts 02215, USA

THE properties of the Moon's rarefied atmosphere, which can be traced through observations of sodium and potassium[1–4], provide important insights into the formation and maintenance of atmospheres on other primitive Solar System bodies[5–7]. The lunar atmosphere is believed to be composed of atoms from the surface rocks and soil, which might have been sputtered by micrometeorites[8], by ions in the solar wind[9], or by photons[10,11]. It might also form by the evaporation of atoms from the hot, illuminated surface[10,11]. Here we report the detection of sodium emission from the Moon's atmosphere during a total lunar eclipse (which occurs when the Moon is full). The sodium atmosphere is considerably more extended at full Moon than expected—it extends to at least nine lunar radii—and its brightness distribution is incompatible with sources involving either solar-wind or micrometeorite sputtering. This leaves photon sputtering or thermal desorption as the preferred explanations for the lunar atmosphere, and suggests that sunlight might also be responsible for the transient atmospheres of other primitive bodies (such as Mercury).

To test hypotheses about the source of the lunar atmosphere, observations under different lunar phase conditions are required to help sort out geometrical factors that link sources and resultant morphologies. For example, the Earth's magnetosphere shields the lunar regolith from direct solar-wind impact for the three to four days spanning full Moon each month. Potter and Morgan[9] reported spectroscopic observations that suggested a dramatic decrease in the sodium brightness at low altitudes (<100 km above the surface) during periods near full Moon, thereby implying that the solar-wind-sputtering source is very important.

Whereas high-resolution spectroscopy and very narrow field (3–4 arcmin) imaging[12] can monitor the sodium distribution close to the Moon under essentially all lunar phase conditions, this is not the case for wide-angle (6–7°) two-dimensional-imaging investigations of the extended atmosphere. With our technique of keeping the disk of the Moon behind an occulting mask and using ~14-Å-wide interference filters, successful images have been obtained only on days near quarter Moon[13]. For the crescent Moon (new±three days), bright sky conditions due to the Moon's proximity to the Sun and long path lengths through the terrestrial atmosphere have, to date, prevented acquisition of images. Under full-Moon conditions, scattered light from the terrestrial atmosphere is simply too strong and attempts to obtain wide-field images have not been successful.

Faced with the severe observational restrictions imposed by scattered light, we recently examined the possibility of acquiring images of the lunar atmosphere under full-Moon conditions when the lunar surface is in the Earth's shadow, but the sodium atmosphere is still in sunlight. This is the situation during the total phase of a lunar eclipse; scattered moonlight ceases to be a problem (the brightness of the eclipsed Moon is at least 10^4 times fainter than the full Moon), and thus the extended lunar atmosphere becomes visible in much the same way as a solar eclipse reveals the corona. An opportunity to test this approach occurred on 29 November 1993 when a total lunar eclipse occurred near zenith at the McDonald Observatory in Fort Davis, Texas.

Figure 1 shows the geometry of the eclipse as viewed from that site. During the total phase, a sequence of in-band ($Na\ D_1 + D_2$) images at 5,893±7 Å and out-of-band (6,200 Å) images were taken. Exposure times using a bare CCD detector were 10 min 13 s, commencing at 06:02:33 UT and 06:16:15 UT, respectively. As described in our previous work[14,15], the in-band image includes sodium from terrestrial and lunar sources, plus scattered light, whereas the out-of-band image shows scattered light. A subtraction yields sodium-only results, but from both lunar and terrestrial regions. A similar image subtraction, taken with the telescope not pointing at the Moon, shows the terrestrial sodium, and hence a final subtraction yields the circumlunar sodium distribution. In addition to standard dark-noise and flat-field corrections, and unique to an eclipse observation, a correction for the penumbral light curve was applied, as sodium atoms are made visible by resonantly scattered sunlight that decreases in intensity from the outer to inner edges of the penumbral region. The final processed image, photometrically calibrated in units of Rayleighs (R), is shown in Fig. 2.

There are several important features in Fig. 2. First, the size of the lunar sodium atmosphere is clearly detectable out to ~9 lunar radii (R_L), a factor of two larger than obtained for the coma under quarter-Moon conditions[15]. At these large distances, the coma exhibits radial symmetry, as shown in fixed radial scan plots below the image. There is a slight asymmetry seen at closer radial distances, but small uncertainties in a host of image-processing corrections (for example, a gradient in the brightness of the terrestrial sodium layer) cause us (at present) to attribute no scientific importance to departures from azimuthal symmetry.

At two positions in the radial scan plots, radial power-law fits to the brightness patterns are given. Under full-Moon conditions, the solar zenith angle $\chi = 90°$ at all locations along the limb, a condition existing only at the poles under quarter-Moon phase. For the eclipse case, the derived equivalent brightness for a light ray just grazing the lunar limb is ~1 kR, with a radial power-law index of ~2. These are remarkably close to the average results at $\chi = 90°$ for the quarter-Moon case[15]. Thus although the full-Moon peak brightness levels are considerably lower than those at the sub-solar point at quarter Moon (by a factor of 7), it appears that this is primarily a solar zenith angle and viewing geometry result, and not one caused by the terrestrial magnetosphere's shielding of solar-wind-induced sputtering sources.

The result presented here is in marked contrast to recent findings, including unpublished observations during this eclipse (A. Potter, personal communication), that point to a very significant

decrease in sodium brightness levels under full-Moon conditions. It is tempting, at first, to seek a reconciliation of these divergent views by considering the altitudes sampled. The Potter and Morgan results[9] come from altitudes very close to the limb (average height, 40 km), whereas the imaging data shown here start at a height of $0.5R_L$ (~800 km) and extend to $\sim 9R_L$ (~14,000 km above the surface). For a solar-wind source turned off by the Moon's entry into the magnetosphere, Na atoms near the surface might show an immediate decrease (and remain low for three to four days), while Na atoms aloft at great distances would persist. Yet Na is destroyed by photoionization, having a lifetime of only ~14 h at 1 AU, and thus it is difficult to attribute the large, bright coma in Fig. 2 to a source that has been 'off' for approximately two days. We conclude that the solar-wind-sputtering source cannot be the dominant agent for the production of the extended lunar atmosphere. As discussed below, the near-Moon sodium may be dominated by a population of cool atoms whose trajectories would all be behind the occulting mask in our observations. Such a component might well decrease appreciably near the solar terminator, leaving the more energetic, sputtered, atoms to reach to the greater distances sampled by our system[11].

We now consider the implications of our observations for the understanding of transient atmospheres in the Solar System. As suggested above, solar-wind sputtering cannot be the dominant agent for the production of the extended lunar atmosphere, simply because the lunar Na coma persists when the Moon is shielded from solar plasma during its passage through the Earth's magnetosphere. The implications for Mercury are straightforward: Mercury has its own magnetosphere to deflect the solar wind, and thus micrometeors, or photosputtering and thermal desorption, remain as possible sources for its atmosphere. Micrometeor sources can be dealt with using the lunar case. Although Monte Carlo simulations show that sources that are spatially uniform[16,17] or dependent on solar zenith angle[18]

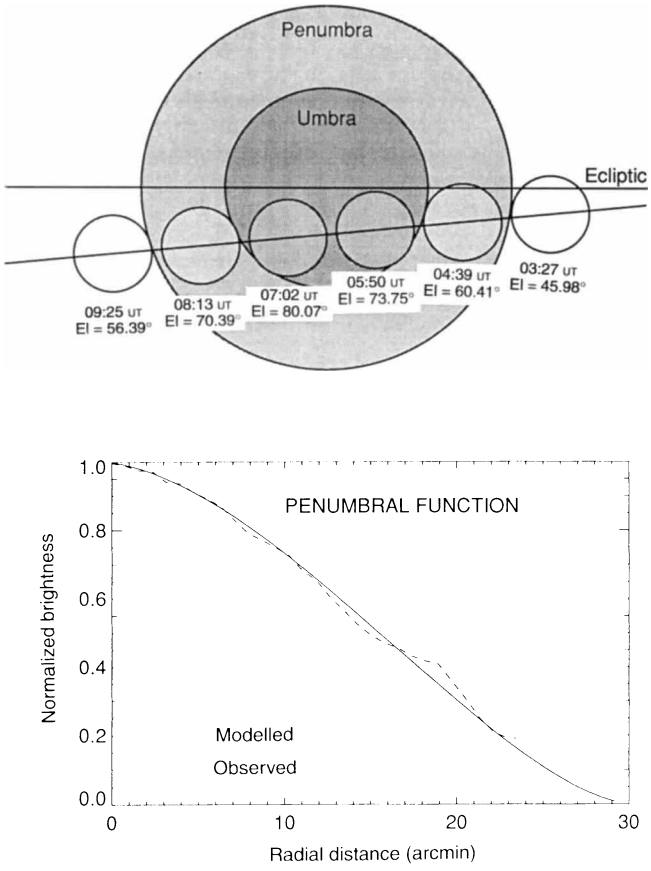

FIG. 1 Top, geometrical and temporal parameters associated with the total lunar eclipse of 29 November 1993, as viewed from the McDonald Observatory (El is the elevation angle of the centre of the Moon). With almost no sunlight to illuminate sodium atoms within the umbra, there are no usable data from that region. Bottom, in the penumbra, the intensity of sunlight increases to 100% along radial lines from the centre of the umbra (the horizontal axis gives the radial distance from the outer to the inner edge of the penumbra). The observed Na brightness needs to be amplified by this penumbral light function to give the true morphology in the absence of an eclipse. This required function was obtained observationally by dividing a white-light image of the Moon taken when it spanned the penumbra by an image of the fully illuminated disk when the Moon was beyond the umbra, that is, at approximately 08:15 and 09:25 UT. Numerically, this function can also be obtained by having a circular Earth eclipse a solar disk of unit intensity, but with a limb darkening pattern of $1-u[1-\cos\theta)$, where $u=0.6$ and $\theta=0$–90° from the centre to the edge of the Sun's disk[22]. Both of these methods gave similar results, as shown, and thus the modelled penumbral function was used to correct those portions of the image affected by the penumbra. Not wanting to amplify any observation by more than a factor of ten, we do not portray results >27 arcmin into the penumbra, where the penumbral light function is <0.1.

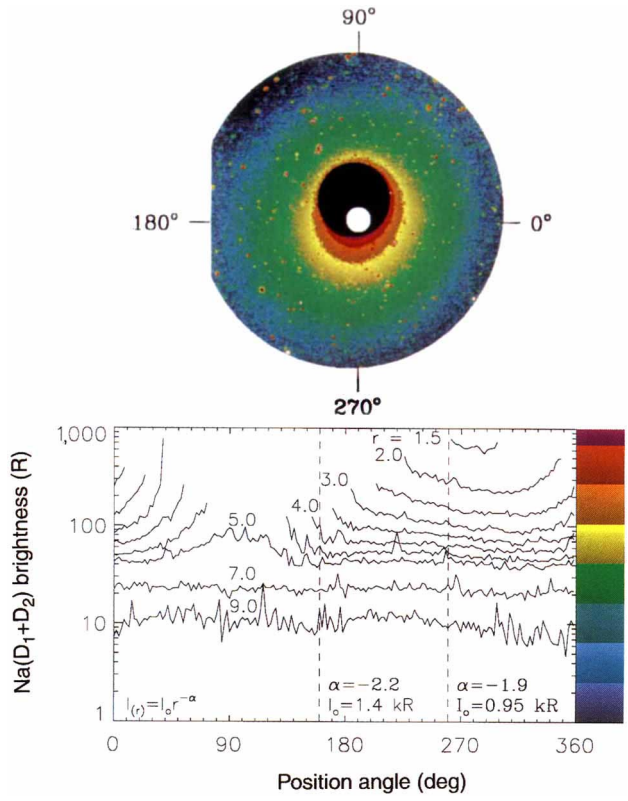

FIG. 2 Top, Sodium brightness surrounding the Moon as obtained during the total phase of the lunar eclipse of 29 November 1993. The dark region in the centre eliminates data from a region where the penumbral function is ≤10%. The position of the obscured lunar disk is given by the white circle region. The brightness levels are displayed in units of Rayleighs (R), with the colour-coded scale given in the bottom panel. Bottom, brightness scans of the eclipse image at fixed radial distances from 1.5 to 9 lunar radii (R_L) using the position angle system depicted in the top panel. The various offsets of the Moon with respect to the occulting mask and the positions of the umbra and penumbra do not allow for complete azimuthal coverage at all radial distances. Power-law representations of the radial pattern are illustrated at two positions (160° and 260°), showing that the basically symmetrical brightness pattern can be described as $I(r)=I_0r^{-\alpha}\approx 1kR/r^2$ (where r is given in units of lunar radii, and I_0 is the equivalent brightness at the limb).

can account for the macroscopic effects of a large coma and tail, the uniform-source calculations do not reproduce the observed patterns at quarter Moon[18]. Thus, micrometeors (if assumed to be a uniform source[8,16,17]) can be eliminated. An influx that varies with latitude and/or local time, as observed on Earth[19], remains to be examined.

The photosputtering and thermal-desorption mechanisms are driven by sunlight. Thermal desorbed atoms are expected to have low speeds corresponding to typical surface temperatures (~350 K), whereas sputtered atoms would have higher, suprathermal (~2,000 K) speeds. Thermal and suprathermal sources would result in atmospheres close to the surface and extended from it, respectively. Such sources act only on the Sun-facing side of the Moon, and they have a solar-zenith-angle dependence: they are greatest at the subsolar point and decrease towards the limb. Compelling arguments have been given that they both act in a 'competing release mechanisms' model[10,11]. Surface temperatures decrease away from the subsolar point, leading to low thermal source efficiencies near the limb (at the poles for quarter Moon, and all around the disk at full Moon), in agreement with observations close to the surface. The suprathermal component responsible for the extended atmosphere cannot be uniform as a source peaked at the subsolar point is clearly required to account for the quarter-Moon patterns[18]. Although details of a photosputtering source are still not fully known, and more observations are needed to clarify the behaviour of competing hot and cold mechanisms[11,12], our wide-field observations find the photosputtering mechanism to be an adequate framework in which to account for the morphologies of the sodium atmosphere at both quarter Moon and full Moon.

If the Moon and Mercury indeed have similar surface materials, then photosputtering applied to the planet's dayside, where solar-wind particles cannot hit directly, would produce a source that increases as the inverse square of distance from the Sun (that is, from 1 AU for the Moon to ~0.4 AU for Mercury), resulting in a source at Mercury ~7 times greater than at the Moon. Moreover, the source at Mercury itself would vary as r^{-2} (where r is Mercury's distance from the Sun) due to the planet's elliptical orbit. Support for both effects is given in separate Monte Carlo simulation studies recently published[17,20]. We suggest here that a long-sought-after synthesis of observations and models linking the two bodies[21] indeed points to surface erosion mechanisms initiated by sunlight as the unifying approach to understanding their transient atmospheres. □

Received 15 May; accepted 31 August 1995.

1. Potter, A. E. & Morgan, T. H. *Science* **241,** 675–680 (1988).
2. Potter, A. E. & Morgan, T. H. *Geophys. Res. Lett.* **15,** 1515–1518 (1988).
3. Tyler, A., Kozlowski, R. & Hunten, D. *Geophys. Res. Lett.* **15,** 1141–1144 (1988).
4. Morgan, T. & Stern, S. A. *Eos* **72,** 225–228 (1991).
5. Sprague, A. L. *Icarus* **84,** 93–105 (1990).
6. A'Hearn, M. & Feldman, P. D. *Icarus* **98,** 54–60 (1992).
7. Hall, D. T., Strobel, D. F., Feldman, P. D., McGrath, M. A. & Weaver, H. A. *Nature* **373,** 677–679 (1995).
8. Morgan, T. & Shemansky, D. *J. geophys. Res.* **96,** 1351–1367 (1991).
9. Potter, A. E. & Morgan, T. *Geophys. Res. Lett.* **21,** 2263–2266 (1994).
10. Kozlowski, R. W. H., Sprague, A. L. & Hunten, D. M. *Geophys. Res. Lett.* **17,** 2253–2256 (1990).
11. Sprague, A., Kozlowski, R., Hunten, D., Wells, W. & Grosse, F. *Icarus* **96,** 27–42 (1992).
12. Stern, S. A. & Flynn, B. C. *Astr. J.* **109,** 835–841 (1995).
13. Mendillo, M., Flynn, B. & Baumgardner, J. *Adv. Space Res.* **13,** 313–319 (1993).
14. Mendillo, M., Baumgardner, J. & Flynn, B. *Geophys. Res. Lett.* **18,** 2097–2100 (1991).
15. Flynn, B. & Mendillo, M. *Science* **261,** 184–186 (1993).
16. Ip, W.-H. *Geophys. Res. Lett.* **18,** 2093–2096 (1991).
17. Smyth, W. H. & Marconi, M. L. *Astrophys. J.* **443,** 371–392 (1995).
18. Flynn, B. & Mendillo, M. *J. geophys. Res.* (in the press).
19. Elford, W. G. & Hawkins, G. S. Res. Rep. no. 9 (Harvard Radio Meteor Project, Harvard Univ., 1964).
20. Smyth, W. H. & Marconi, M. L. *Astrophys. J.* **441,** 839–864 (1995).
21. Sprague, A. L. thesis, Univ. Arizona (1990).
22. Papagiannis, M. D. *Space Physics and Astronomy* 94–95 (Gordon & Breach, New York, 1972).

ACKNOWLEDGEMENTS. We thank D. Nottingham for assistance with image processing, and J. Emery for analysis work. M.M. and J.B. are guest observers at the McDonald Observatory in Fort Davis, Texas, and thank their colleagues at the observatory for their cooperation and assistance. We acknowledge referee reports from, and informative discussions with, W. Smyth, A. Potter, A. Sprague and D. Hunten. This work was supported, in part, by NASA and the Center for Space Physics at Boston University.

A geochemical model for the formation of hydrothermal carbonates on Mars

L. L. Griffith & E. L. Shock

Department of Earth and Planetary Sciences, McDonnell Center for the Space Sciences, Campus Box 1169, 1 Brookings Drive, Washington University, St Louis, Missouri 63130, USA

IT IS often argued[1–3] that substantially more carbon dioxide and water were degassed from the martian interior than can be found at present in the atmosphere, polar caps and regolith. Calculations have shown that atmospheric escape cannot account for all of the missing volatiles[4]. Suggestions that carbon dioxide is stored as marine or lacustrine deposits[5], are challenged by Earth-based and spacecraft remote-sensing data[6,7]. Moreover, recent modelling of the martian atmosphere suggests that rainfall or open bodies of water are in any case unlikely to have persisted for extended periods of time[8,9]. Hydrothermal carbonates therefore provide a possible solution to this dilemma. Using an accessible terrestrial system (Iceland) as a guide to the underlying processes, and a host rock composition inferred from the least-altered martian meteorite[10], we present a geochemical model for the formation of carbonates in possible martian hydrothermal systems. Our results suggest that an extensive reservoir of carbonate minerals—equivalent to an atmospheric pressure of carbon dioxide of at least one bar—could have been sequestered beneath the surface by widespread hydrothermal activity in the martian past.

Hydrothermal systems are an inevitable consequence of igneous activity occurring in the presence of liquid water, and they have presumably existed on Mars, powered by heat from volcanic intrusions and possibly by impact events[11]. Direct analysis of martian hydrothermal systems is not possible at present, but the study of active, accessible and diverse terrestrial systems, such as those in Iceland, can considerably expand our understanding of martian systems and influence exploration plans.

In Iceland, hydrothermal circulation systems are deep and widespread. The source of water for systems in the interior of the island is meteoric. This relatively fresh water interacts with basaltic host rock at temperatures to at least 340 °C (refs 12, 13). These systems are well characterized chemically, mineralogically and physically, as summarized in Fig. 1, which shows the generalized petrogenetic sequence of the observed alteration minerals found in basalt-hosted systems throughout Iceland as a function of temperature[12–17]. Calcite is present over the entire temperature range of alteration. Hydrothermal carbonate deposits in Iceland range from ~1 to ~30 vol.% of the altered rock, with an average of approximately 4% (ref. 18). Carbonates are found as vein-filling materials and mineral replacements, and are located at least as deep as the deepest well (~2 km below the present surface)[14,15]. The distribution and ubiquity of the deposits imply that a great deal of carbon dioxide is concealed below the surface as hydrothermal deposits. Assuming 50% alteration to a depth of 5 km and 4 vol.% carbonate in the alteration, we estimate that a likely inventory of CO_2 sequestered within Iceland is ~2.5 mbar or about 6 times the 0.4 mbar of CO_2 in Earth's present atmosphere. This entire amount of CO_2 would have been sequestered over only the past 16 Myr, Iceland's lifetime[14]. This calculation demonstrates that hydrothermal systems, even on a small scale, can greatly affect a planet's CO_2 inventory.

To consider the generation of Icelandic deposits in more detail, we have pursued a series of reaction-path calculations[19] involving host rock composition, temperature, water:rock (W/R) ratio, and carbon dioxide fugacity as variables. These calculations start with a system far from equilibrium and use